Applied Physics A (2022) 128:1104
https://doi.org/10.1007/s00339-022-06260-y

Applied Physics A
Materials Science & Processing

Performance analysis of dielectric modulated underlap FD-SOI MOSFET for biomolecules detection

Saurabh Kumar[1] · **R. K. Chauhan**[1]

Received: 6 September 2022 / Accepted: 14 November 2022 / Published online: 22 November 2022

Abstract

Effective biosensors are required to detect contagious viruses through a rapid test kit using electronic components. Field-effect transistor-based biosensors have been identified as potential candidates for label-free and rapid sensing applications. In this work, a dielectric modulated (DM) two-side underlap gate (*U*) Field-Effect Transistor (FET) biosensor device with a single gate structure is investigated for the label-free electrical detection of biomolecules. For detecting the presence of biomolecules immobilized in the underlap region, the change in subthreshold slope (SS), ON current (I_{ON}), ON current, OFF current ratio (I_{ON}/I_{OFF}), and transconductance (gm) of the device have been considered. The proposed device is investigated for different underlap lengths, and its impact on device sensitivity is analyzed. All the characteristic trends have been validated through device simulation.

Keywords Dielectric modulation · Biomolecules · Biosensor · Underlap region · Cavity region

1 Introduction

In the present scenario, different viruses are a primary concern worldwide. For this, the detection of the protein and DNA of the virus is essential. Different researchers worldwide are developing a cost-effective, accurate, and high-performance biosensor. Many of them have developed biosensors to detect various viruses and proteins. Clark introduced the first biosensor in 1962 [1], which was later employed in various applications like the detection of the virus [2], toxicity [3], cancer [4], and can be used for health prognosis [5, 6], etc. Biosensors convert biological responses into electrical signals [7], and it works by combining two basic components, biological receptors and physical–chemical transducers [8]. The biological receptor converts the responses from the biochemical domain to a physical or chemical output signal with a defined sensitivity. Transducers convert this chemical or physical output signal to the electrical domain [8]. Bergveld, in 1970, invented ISFET, which started the use of FET for various biosensor applications [9].

The multiple benefits that can be achieved with such a design have recently boosted interest in using a field-effect transistor (FET) for various biosensors [10–19]. Janata and Caras, in 1980, used a FET biosensor for penicillin, showing the first practical uses of a FET biosensor [20]. Many other papers demonstrate FET biosensors' capabilities with different molecular targets [21], like nucleotides, cells [22], and amino acids [23]. These three papers [21–23] are based on experimental work. Rahman et al. simulated the junctionless double-gate MOSFET and its performance is analyzed. The device can be used to identify biomolecules like deoxyribonucleic acid (DNA), enzymes, cells, etc. [24]. The impact on sensitivity is seen by changing the biomolecule's position. Singh et al. simulated the $Si_{0.5}Ge_{0.5}$ Source dual-electrode doping less tunnel FET (DEDLTFET) biosensors and study the effect on performance by changing the cavity length, charge density (QF) and cavity thickness [25]. Kalra et al. worked on the tunability of the sensing performance of a FET biosensor by using electrostatic gating of the metal–semiconductor junction [26]. Hwang et al. explained using FET with a deformed monolayer graphene channel to detect nucleic acid [27]. All the above authors are trying to achieve better sensitivity for the proposed biosensor by using different structures and materials, but there

✉ Saurabh Kumar
saurabh.k2u@gmail.com

R. K. Chauhan
rkchauhan27@gmail.com

[1] Department of Electronics & Communication Engineering, Madan Mohan Malaviya University of Technology, Gorakhpur, Uttar Pradesh 273010, India

is a limitation of sensitivity, as can be analyzed from their work, and also complex structure causes a difficult fabrication process [28]. Lower leakage current, better control over the channel, electrical insulation of substrate, fewer photolithography steps, and direct adaptation of the bulk IC design method are some advantages of using silicon on insulator (SOI) MOSFET [29–34]. In fully depleted SOI (FD-SOI) MOSFET, the parasitic capacitance between the source and drain, as exhibited by the bulk transistor, is reduced, which helps to provide better performance [35].

This manuscript proposes a dielectric modulated two-side underlap FET biosensor device (DMUFET) with a single gate structure to detect the biomolecule. The proposed device incorporated biomolecules as a biosensing material. The proposed biosensor's electrical response is analyzed by changing the dielectric constant of biomolecules in the underlap region. In addition, the change in sensitivity of SS, I_{ON}, I_{ON}/I_{OFF}, and gm with respect to various dielectric constants are analyzed and discussed. Moreover, a comparison of sensitivity is also shown in the manuscript by varying the length of underlap region.

2 Device architecture and simulation

The Atlas SILVACO 2D device simulator is used for all the device simulations. The device parameter, its dimension value, and doping concentration for source, drain, and channel, which are used for simulation, are stated in Table I. The proposed biosensor device architecture and calibrated drain current characteristics curve are depicted in Fig. 1a, b. In Fig. 1a, Lu is the underlap region length, and Lg is the gate length. The thickness of the underlap region in which biomolecules are immobilized is considered 15 nm, the thickness of the oxide layer (SiO_2) just above the channel is 5 nm, the thickness of the chromic oxide (Cr_2O_3) just below the gate is considered as 15 nm, and metal work function is considered as 5.1 eV. Properties of chromic oxides, such as low dielectric loss, high oxidation resistance, and high melting temperature, make it a better choice to be used as gate dielectric material in FETs than other high K materials [36, 37]. The SiO_2 layer between the air and the silicon region is regarded under the cavity region. The presence of charges in the biomolecules significantly affects the biosensing action. However, for this work, two distinct oxide materials that have been used are Cr_2O_3 and SiO_2, where SiO_2 has low permittivity compared to Cr_2O_3. These two-oxide material stacking configurations can be chosen to reduce the interfacial trap density, which improves the device's performance [38, 39]. The open cavity region (underlap region) is used for sensing the immobilized biomolecules. The biomolecules are introduced in the underlap region by increasing the dielectric constant, i.e., $K > 1$. Many works of literature reported that biomolecules like protein, biotin, streptavidin, and APTES have a dielectric constant of 2.50, 2.63, 2.1, and 3.57, respectively [40–42]. The proposed biosensor's sensitivity is assessed at $V_{DS} = 0.5$v and $V_{GS} = 1.5$v (bias condition).

The various model, such as Field-Dependent Mobility Model (FLDMOB), Shockley–Read–Hall (SRH) Recombination Model, Concentration Dependent Mobility Model (CONMOB), Bandgap Narrowing Model (BGN), and Auger Model (AUGER) present in Atlas SILVACO tool has been used to simulate the electrostatic and current of the device [43]. The newton trap numerical solver is used during simulation to avoid convergence issues in the SOI structure [43].

3 Results and discussion

The Gate voltage (V_{GS}) vs. Drain current (I_D) plot is depicted in Fig. 2a. The figure reveals that the drain current reduces as the device's underlap length (Lu) increases. This reduction in drain current is due to the increase in series resistance introduced due to the increase in underlap length [44]. This restricts the inversion layer formation

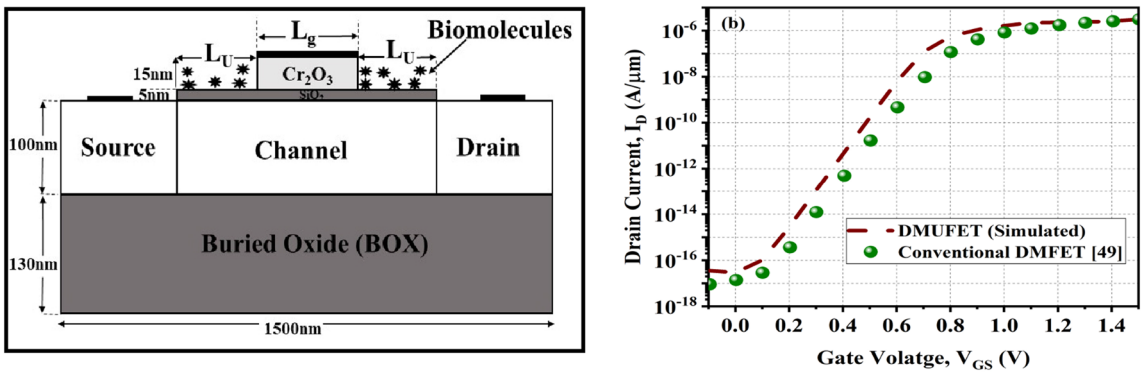

Fig. 1 (**a**) Proposed device structure (DMUFET) and (**b**) calibrated DMUFET I_D characteristics compared with conventional DMFET

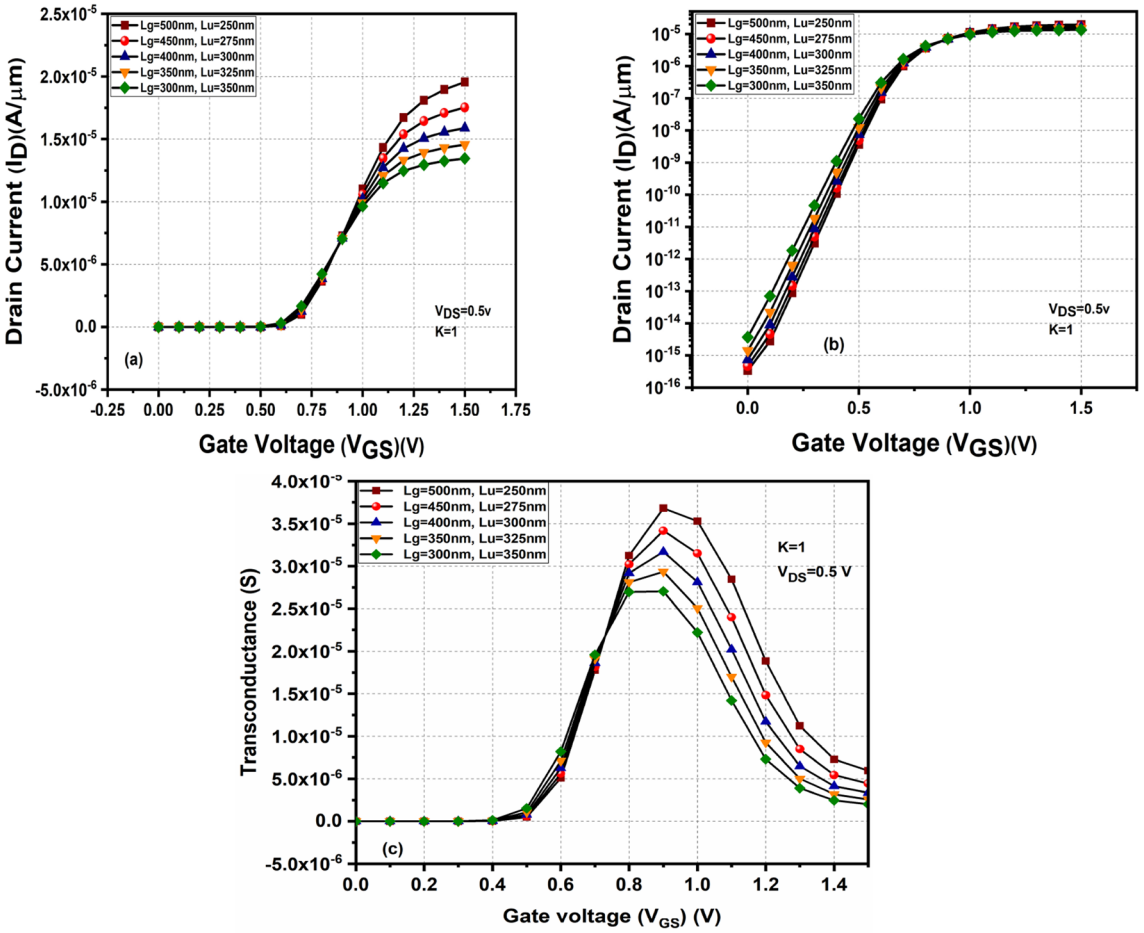

Fig. 2 (**a**) I_D–V_{GS} characteristics of DMUFET, results of simulation with $K=1$ (air), (**b**) subthreshold drain current with gate voltage, (**c**) transconductance with gate voltage for different gate and underlap length

after gate voltage is applied, thus reducing the drain current. The underlap length is increased up to 350 nm, while the gate length (Lg) reduces to 300 nm, due to which controlling the channel becomes more difficult, which increases the leakage current or off current as depicted in Fig. 2b. The analysis is done keeping $V_{DS}=0.5$v, $V_{GS=}1.5$v, and the underlap length is filled with air ($K=1$). Figure 2c shows the change in transconductance with different gate lengths and underlap lengths. The graph clearly shows that the transconductance improves as the gate length increases due to an improved drain current. The device's efficiency in converting the gate voltage into drain current is provided by transconductance [45].

$$g_m = \frac{\partial I_D}{\partial V_{GS}}. \tag{1}$$

An increase in transconductance (g_m) indicates high sensitivity for biomolecules. From Fig. 2c, the transconductance peak is observed at 0.9 Volts (V_{GS}), which suggests that an improved sensitivity can be achieved at this biasing condition.

Figure 3 depicts the variation of an electric field, surface potential, energy band diagram, and electron concentration along the lateral length of the device when biomolecules are immobilized in the cavity region. Lu = 350 nm and Lg = 300 nm are selected for simulation since this is the optimum value for maximum device sensitivity. The surface potential is at the highest level for the empty cavity region, i.e. ($K=1$). The surface potential of underlap section shifts downwards with the increase in biomolecules dielectric constant from one to a higher value, as shown in Fig. 3a. Figure 3b shows that the electric field is higher at the gate-underlap junction when air is immobilized in the cavity region ($K=1$). The plot of energy band diagram variation with different dielectric constant values is shown in Fig. 3c, which indicates an energy band diagram rise for the higher dielectric constant value at the underlap region. In Fig. 3d, the electron concentration of the cavity region reduces as the constant dielectric increases, which is why

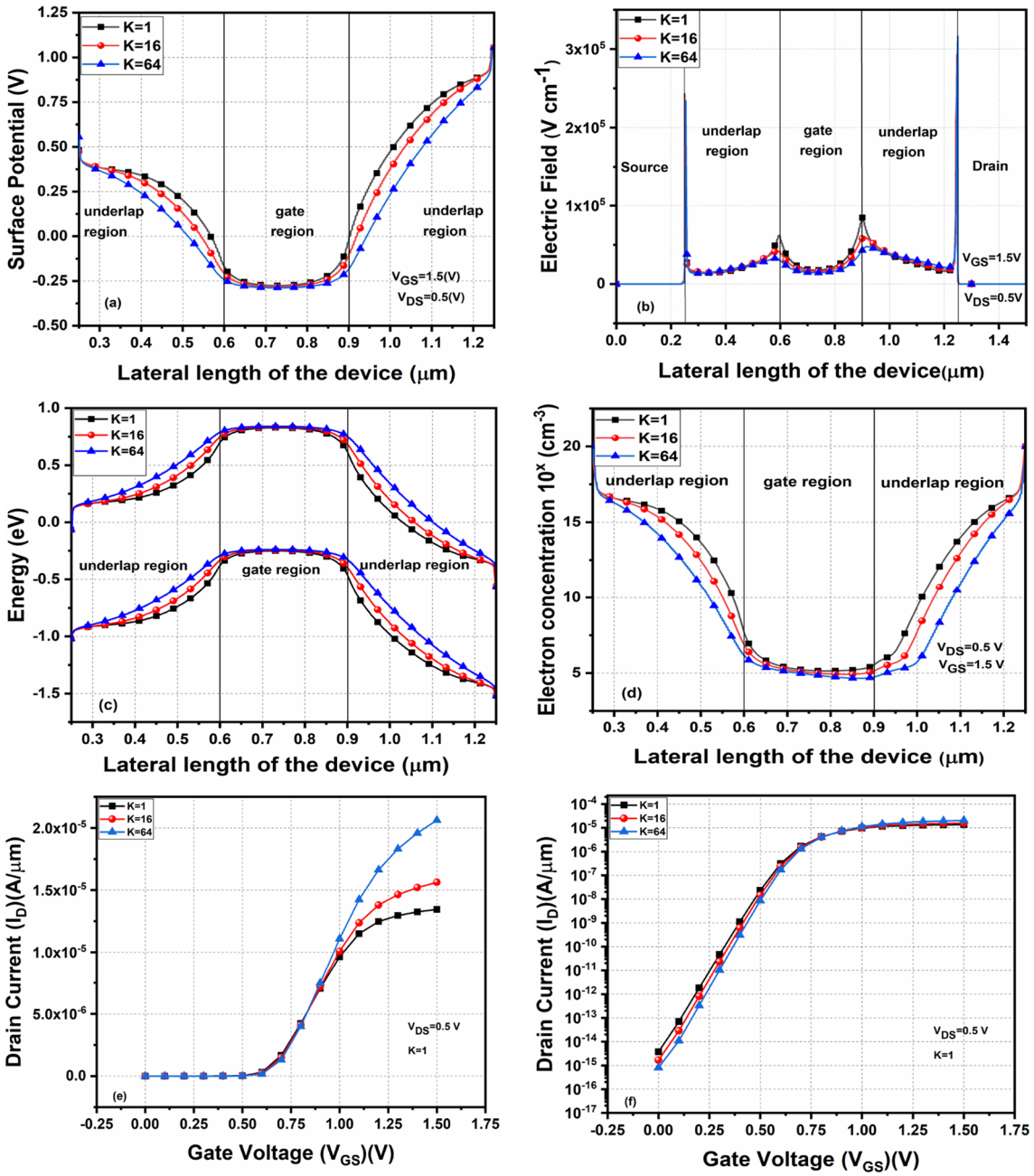

Fig. 3 Effect of varying dielectric constant on the (**a**) surface potential, (**b**) electric field, (**c**) energy band diagram, and (**d**) electron concentration along the lateral length of the device. Effect of varying dielectric constant on (**e**) drain current and (**f**) subthreshold drain current

surface potential shifts downwards in the cavity region as the K value increases. Figure 3e, f shows the I_D–V_{GS} characteristics on a linear scale (drain current) and on a log scale (subthreshold drain current), respectively. In both the figure, it is visible that the drain current improves with the increase in dielectric constant, and the subthreshold leakage current reduces with the increment in dielectric constant, so it can be analyzed that the I_{ON}/I_{OFF} ratio is high for higher dielectric constant.

The DNA biomolecules are charged particles; therefore, for the detection of DNA, the impact of a charged biomolecule on the DMUFET biosensors is analyzed. The presence of charges in biomolecules affects the biosensing action of the DMUFET biosensor. $L_u = 350$ nm and $L_g = 300$ nm are selected for simulation since this is the optimum value for maximum device sensitivity. The effect of charged biomolecules on the surface potential of the DMUFET biosensor is presented in Fig. 4a. It is reflected from the figure

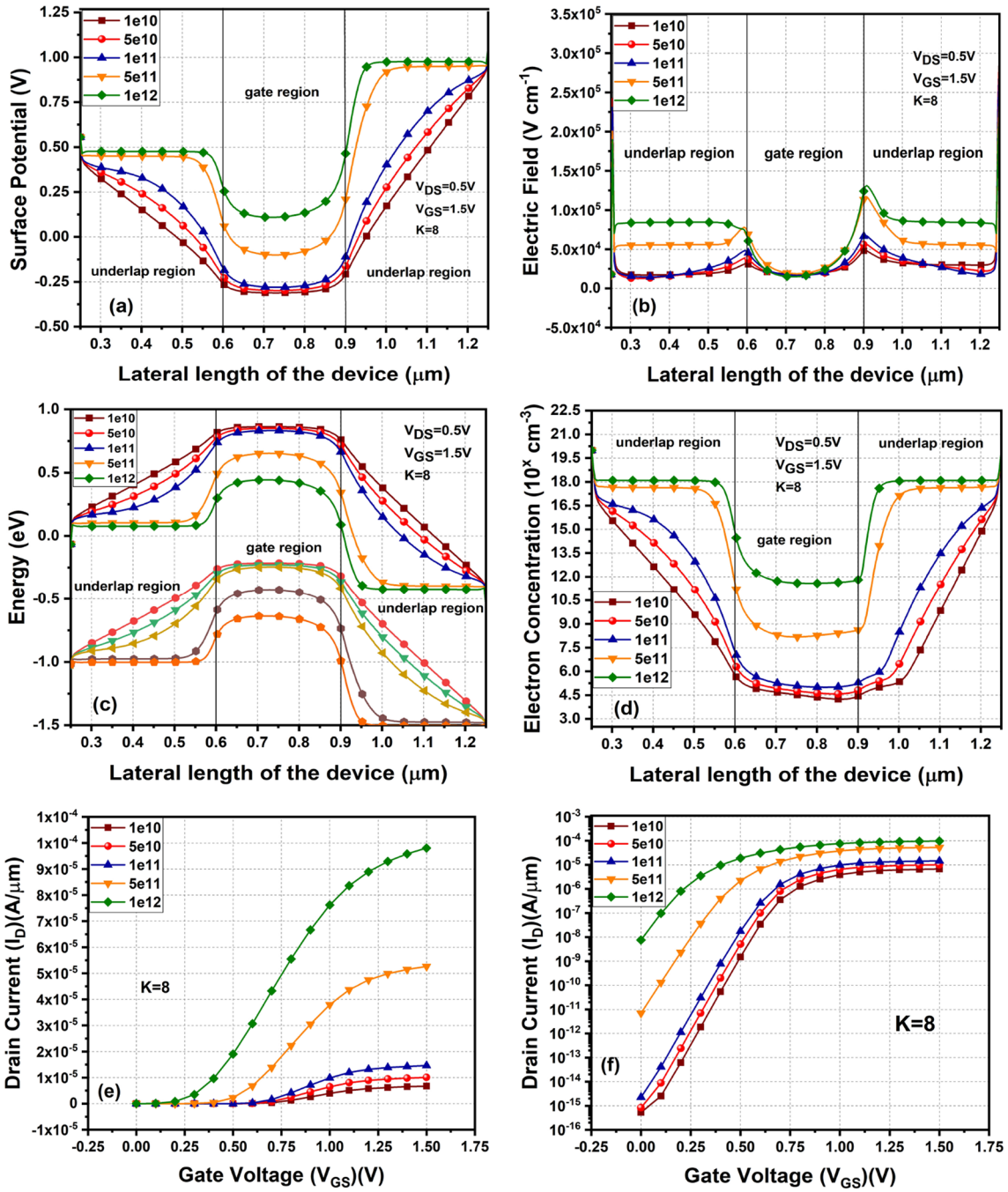

Fig. 4 Effect of varying interface charge density on (**a**) surface potential, (**b**) electric field, (**c**) energy band diagram, and (**d**) electron concentration along the lateral length of the device. Effect of varying interface charge on (**e**) drain current (**f**) subthreshold drain current

that as the positive charge biomolecules are greater than before in the cavity, the surface potential shift upwards due to flat band voltage alteration. It makes the threshold voltage of the device to be lesser. The electric field increases with the positivity of charged biomolecules from $1e^{10}$ C/cm^2 to $1e^{12}$ C/cm^2 in the underlap region, as depicted in Fig. 4b. Figure 4c shows the variation in the energy band diagram with increased positivity of charged biomolecules; the figure clearly shows that the energy band diagram shifts downwards. As shown in Fig. 4d, the electron concentration of the cavity region improves as the positivity of charged biomolecules increases. That is why surface potential shifts upwards in the cavity region with the rise in the positivity of charged biomolecules. Drain current for different V_{GS} in the presence of positively charged biomolecules is shown in Fig. 4e. This can be undoubtedly inferred from the graph

that with the rise in the positivity of biomolecule from $1e^{10}$ C/cm^2 to $1e^{12}$ C/cm^2, the number of electrons in the channel region has improved significantly to a prominent attraction force. Hence, the I_{ON} has also been enhanced by a noticeable margin. Figure 4f shows the transfer characteristics of the device on the binding of the charged biomolecules for positively charged analytes OFF current rise.

From Figs. 3 and 4, it can be analyzed that the dielectric constant is less dominating than the charge effect. The impact of charge variation is more as compared with the dielectric constant variation on different parameters.

3.1 Sensitivity analysis

Percentage sensitivity analysis when biomolecules are immobilized in the gate-underlap section is done by the mathematical formulae as expressed [45].

$$\%Sensitivity = \left|\frac{(V1 - V2)}{V1}\right| \times 100. \quad (2)$$

$V1$ is the value of quantity when underlap region is filled with air ($K=1$), and $V2$ is the value of quantity when underlap region is filled with the biomolecule (K value other than 1). Equation 2 expresses the absolute percentage deviation in the electrical parameters of the sensor with respect to air when the underlap region is immobilized with biomolecules (Table 1).

In biosensors based on FET, the I_{ON}/I_{OFF} is also utilized as the sensing parameter to notice the sensitivity of the biosensor device when biomolecules are introduced into the device. Figure 5 shows that the absolute percentage sensitivity of SS improves with the increase in dielectric constant and the increase in underlap length. Figure 5a shows the percentage sensitivity of SS for different dielectric constants with various gate and underlap lengths. The SS sensitivity is maximum with Lu = 350 nm and Lg = 300 nm. Figure 5b shows the percentage sensitivity of ON current, which indicates the increase in ON current sensitivity with different dielectric constants. Figure 5b depicts that the sensitivity is better for underlap of 250 nm length, which means that the sensitivity for ON current is better for smaller underlap length and larger gate length, i.e. (Lu = 250 nm and Lg = 500 nm). This indicates poor control of the device due to a smaller gate length. The increment in OFF current is more significant than the decrement in ON, with the increase in constant dielectric results in better sensitivity in I_{ON}/I_{OFF}, as shown in Fig. 5c. The absolute percentage sensitivity of transconductance increases with the increase in the K value. There is no significant change in percentage sensitivity at a lower dielectric constant for various underlap lengths. Still, the change in sensitivity is visible for a higher dielectric constant, as shown in Fig. 5d.

Table 1 Device parameter used for simulation

S. No	Parameters	Dimension value/doping
1	Source/drain length	250 nm
2	Channel length	1000 nm
3	BOX thickness	130 nm
4	Oxide thickness (SiO_2)	5 nm
5	Oxide thickness (Cr_2O_3)	15 nm
6	Source/drain doping, N_D^+	1×10^{20} cm^{-3}
7	Channel doping, N_A	5.1 eV
8	Gate metal work function	1×10^{15} cm^{-3}

3.1.1 Improvement in sensitivity

Protein and DNA are essential biomolecules in nature. The dielectric constant of protein ranges between 2 and 4 [46, 47]. The dielectric constant of DNA is 8 [48]; therefore, to detect the protein, the K value of biomolecules in the sensing region is considered 2.1, 4.1, and for DNA, it is considered 8. DNA is a charged biomolecule, and sometimes protein also contains a charge, so a fixed charge, $1e^{11}$ C/cm^2, at the Si–SiO_2 interface region is considered. The proposed sensor exhibits a reproducible, specific detection of proteins and DNA, as shown in Fig. 6, showing potential for detecting viruses and cancer markers [49]. As shown in Fig. 6, the proposed sensor with underlap length of 350 nm showed improvement in sensitivity compared to underlap length of 250 nm for different dielectric constants. Underlap length of 350 nm shows 3.4 percent improvement in I_{ON}/I_{OFF} sensitivity for dielectric constant ($K=2.1$), it shows 28.9 percent improvement in I_{ON}/I_{OFF} sensitivity for $K=4.1$, and a percentage improvement of 55.5 in I_{ON}/I_{OFF} sensitivity for $K=8$ compared to 250 nm underlap length. This result indicates that more cavity regions contribute to better sensitivity, and the sensitivity is more elevated for a higher dielectric constant.

4 Conclusion

This manuscript shows a conclusive effect of increasing or decreasing the cavity region length. The increase in cavity region length provides more space for biomolecule immobilization, hence increased sensitivity. A decrease in underlap length results increase in gate length, which offers improved control over the channel, due to which the leakage current decrease (I_{OFF} decreases). From the analysis, it can be determined that the sensitivity of the proposed device can be enhanced by increasing the underlap length where the biomolecules are immobilized. Changes in surface potential, energy band diagram, electric field,

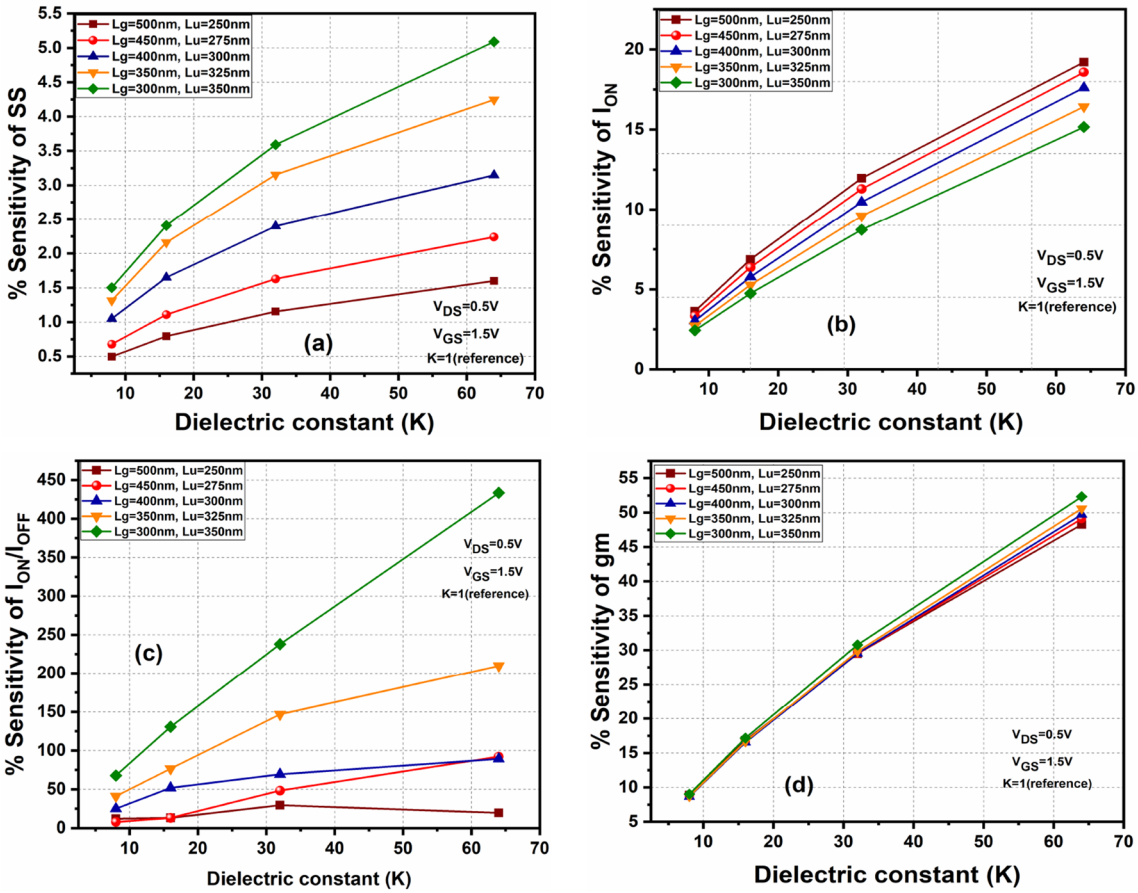

Fig. 5 Absolute percentage sensitivity variation of (**a**) subthreshold slope, (**b**) ON current, (**c**) ON current OFF current ratio, and (**d**) transconductance with a different dielectric constant for various gate and underlap lengths

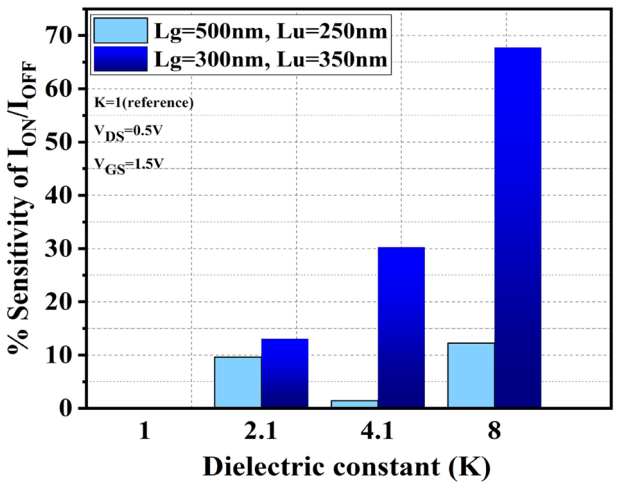

Fig. 6 Comparison of the absolute percentage sensitivity of I_{ON}/I_{OFF} for underlap lengths 250 nm and 350 nm

electron concentration, drain current, and subthreshold drain current has been inspected in-depth during the biomolecule's detection. From the analysis, it has been found that the sensitivity of the biosensor device is enhanced much more by increasing the positivity of charged biomolecules as compared to an increase in the dielectric constant. Also, the absolute percentage sensitivity of SS, I_{ON}, ON, and OFF current ratio and transconductance have been observed in the existence of charged biomolecules for different dielectric constants. The proposed device shows improvement in absolute percentage sensitivity of I_{ON}/I_{OFF} by using 350 nm Lu compared to 250 nm Lu, which is 28.9 percent for $K = 4.1$, and improvement in absolute percentage sensitivity of transconductance is 4 percent for $K = 64$. Therefore, the manuscript clearly states that the suggested biosensor device can be a promising and good substitute for developing advanced and emerging bio-equipment because of its simple structure, higher sensitivity, and less thermal budgeting (low fabrication cost). The simulated results indicate that the proposed DMUFET can detect biomolecules such as protein and DNA. The proposed

device can be a promising candidate to explore further and research label-free biosensing.

Funding The authors declare that no funds, grants, or other support were received during the preparation of this manuscript.

Data availability Data sharing is not applicable to this article as no new data were created or analyzed in this study.

Declarations

Conflict of interest The authors declare that they have no known competing financial interests or personal relationships that could have appeared to influence the work reported in this paper.

Ethical approval This article does not contain any studies with human participants performed by any of the authors.

References

1. L.C. Clark, C. Lyons, Ann. N. Y. Acad. Sci. **102**, 29–45 (1962). https://doi.org/10.1111/j.1749-6632.1962.tb13623.x
2. M. Shariati, Biosens. Bioelectron. **105**, 58–64 (2018). https://doi.org/10.1016/j.bios.2018.01.022
3. H. Gong, F. Chen, Z. Huang, Y. Gu, Q. Zhang, Y. Chen, Y. Zhang, J. Zhuang, Y.K. Cho, R.H. Fang, W. Gao, S. Xu, L. Zhang, ACS Nano **13**, 3714–3722 (2019). https://doi.org/10.1021/acsnano.9b00911
4. D.S. Su, P.Y. Chen, H.C. Chiu, C.C. Han, T.J. Yen, H.M. Chen, Biosens. Bioelectron. **141**, 111209 (2019). https://doi.org/10.1016/j.bios.2019.03.042
5. S.A. Fahliyani, A.A. Rastegari, A.N. Yadav, N. Yadav, New Fut. Dev. Microbial Biotechnol. Bioeng. (2020). https://doi.org/10.1016/b978-0-12-820528-0.00005-3
6. A. Pantelopoulos, N.G. Bourbakis, IEEE Trans Syst. Man Cybern. Part C Appl. Rev. **40**, 1–12 (2010). https://doi.org/10.1109/TSMCC.2009.2032660
7. M. Torequl Islam, J. Gynecol. Womens Health **2**, 2 (2017). https://doi.org/10.19080/jgwh.2017.05.555667
8. N. Bhalla, P. Jolly, N. Formisano, P. Estrela, Essays Biochem. **60**, 1–8 (2016). https://doi.org/10.1042/EBC20150001
9. P. Bergveld, IEEE Trans. Biomed. Eng. **17**, 70–71 (1970). https://doi.org/10.1109/TBME.1970.4502688
10. P. Singh, D.S. Yadav, Appl. Phys. A Mater. Sci. Process. **127**(671), 1–15 (2021). https://doi.org/10.1007/s00339-021-04813-1
11. N.K. Singh, D. Mandal, R. Kar, Appl. Phys. A Mater. Sci. Process. **127**(347), 1–9 (2021). https://doi.org/10.1007/s00339-021-04495-9
12. N.N. Reddy, D.K. Panda, Appl. Phys. A Mater. Sci. Process. **127**(682), 1–9 (2021). https://doi.org/10.1007/s00339-021-04840-y
13. E.A. Kabaa, S.A. Abdulateef, N.M. Ahmed, Z. Hassan, F.A. Sabah, Appl. Phys. A Mater. Sci. Process. **125**(753), 1–10 (2019). https://doi.org/10.1007/s00339-019-3056-0
14. B. Dewan, S. Chaudhary, M. Yadav, Appl. Phys. A Mater. Sci. Process. **127**(791), 1–9 (2021). https://doi.org/10.1007/s00339-021-04933-8
15. M.K. Anvarifard, Z. Ramezani, I.S. Amiri, K. Tamersit, A.M. Nejad, J. Mater. Sci.: Mater. Electron. **31**, 22699 (2020). https://doi.org/10.1007/s10854-020-04795-5
16. M. Kumari, N.K. Singh, M. Sahoo, H. Rahaman, Appl. Phys. A Mater. Sci. Process. **127**(130), 1–8 (2021). https://doi.org/10.1007/s00339-020-04256-0
17. A. Lodhi, C. Rajan, A.K. Behra, D.P. Samajdar, D. Soni, D.S. Yadav, Appl. Phy. A Mater. Sci. Process. **126**(837), 1–8 (2020). https://doi.org/10.1007/s00339-020-04008-0
18. S.I. Amin, L. Gajal, S. Anand, Appl. Phys. A Mater. Sci. Process. **124**(578), 1–8 (2018). https://doi.org/10.1007/s00339-018-2003-9
19. M. Shariati, Appl. Phys. A Mater. Sci. Process. **123**(370), 1–8 (2017). https://doi.org/10.1007/s00339-017-0994-2
20. S. Caras, J. Janata, Anal. Chem. **52**, 1935–1937 (1980). https://doi.org/10.1021/ac50062a035
21. M. Fehr, D.W. Ehrhardt, S. Lalonde, W.B. Frommer, Curr. Opin. Plant Biol. **7**, 345–351 (2004). https://doi.org/10.1016/j.pbi.2004.03.015
22. A.B. Kharitonov, M. Zayats, A. Lichtenstein, E. Katz, I. Willner, Sensors Actuators B Chem. **70**, 222–231 (2000). https://doi.org/10.1016/S0925-4005(00)00573-6
23. C.H. Kim, J.H. Ahn, J.Y. Kim, J.M. Choi, K.C. Lim, T. Jung Park, N. Su Heo, H. Gu Lee, J.W. Kim, Y.K. Choi, Biosens Bioelectron. **41**, 322–327 (2013). https://doi.org/10.1016/j.bios.2012.08.047
24. E. Rahman, A. Shadman, Q.D.M. Khosru, Sens. Bio-Sensing Res. **13**, 49–54 (2017). https://doi.org/10.1016/j.sbsr.2017.02.002
25. A. Singh, S.I. Amin, S. Anand, SILICON **12**, 2301–2308 (2020). https://doi.org/10.1007/s12633-019-00325-z
26. S. Kalra, M.J. Kumar, A. Dhawan, IEEE Sens. J. **20**, 2261–2269 (2020). https://doi.org/10.1109/JSEN.2019.2952333
27. M.T. Hwang, M. Heiranian, Y. Kim, S. You, J. Leem, A. Taqieddin, V. Faramarzi, Y. Jing, I. Park, A.M. van der Zande, S. Nam, N.R. Aluru, R. Bashir, Nat. Commun. **11**, 2 (2020). https://doi.org/10.1038/s41467-020-15330-9
28. N.N. Reddy, D.K. Panda, SILICON **13**, 3085–3100 (2021). https://doi.org/10.1007/s12633-020-00657-1
29. J.P. Celis, B. Prakash, Surf. Process. by Dir. Energy Tech. **2**, 111–119 (2006). https://doi.org/10.1016/B978-008044496-3/50005-8
30. A. Chaudhry, M.J. Kumar, IEEE Trans. Device Mater. Reliab. **4**, 99–109 (2004). https://doi.org/10.1109/TDMR.2004.824359
31. W.Y. Lu, Y. Taur, IEEE Trans. Electron Devices **53**, 1137–1141 (2006). https://doi.org/10.1109/TED.2006.871879
32. K. N. Singh and P. K. Dutta, Proc. 3rd Int. Conf. 2019 Devices Integr. Circuit, Dev 2019, 231–235 (2019). https://doi.org/10.1109/DEVIC.2019.8783714.
33. J.P. Colinge, Microelectron. Eng. **84**, 2071–2076 (2007). https://doi.org/10.1016/j.mee.2007.04.038
34. V.P. Trivedi, J.G. Fossum, IEEE Electron Device Lett. **26**, 26–28 (2005). https://doi.org/10.1109/LED.2004.839624
35. K. Cheng, A. Khakifirooz, Sci. China Inf. Sci. **59**, 1–15 (2016). https://doi.org/10.1007/s11432-016-5561-5
36. C.P. Kwan, R. Chen, U. Singisetti, J.P. Bird, Appl. Phys. Lett. **106**, 1–5 (2015). https://doi.org/10.1063/1.4915309
37. M.M. Abdullah, F.M. Rajab, S.M. Al-Abbas, AIP Adv. (2014). https://doi.org/10.1063/1.4867012
38. S.K. Parija, S.K. Swain, S. Adak, S.M. Biswal, P. Dutta, SILICON (2021). https://doi.org/10.1007/s12633-021-01118-z
39. M. Saxena, S. Haldar, M. Gupta, R.S. Gupta, Solid. State. Electron. **47**, 2131–2134 (2003). https://doi.org/10.1016/S0038-1101(03)00221-1
40. M.S. Parihar, A. Kranti, Nanotechnology **26**, 145201 (2015). https://doi.org/10.1088/0957-4484/26/14/145201
41. K. Talley, C. Ng, M. Shoppell, P. Kundrotas, E. Alexov, PMC Biophys. **1**, 1–23 (2008). https://doi.org/10.1186/1757-5036-1-2
42. M.K. Gilson, B.H. Honig, Biopolymers **25**, 2097–2119 (1986). https://doi.org/10.1002/bip.360251106
43. ATLAS user's manual, SILVACO Int, Santa Clara, CA (2014).

44. J.S. Lee, J.H. Seo, S. Cho, J.H. Lee, S.W. Kang, J.H. Bae, E.S. Cho, I.M. Kang, Curr. Appl. Phys. **13**, 1143–1149 (2013). https://doi.org/10.1016/j.cap.2013.03.012
45. S. Kumar, R.K. Chauhan, M. Kumar, SILICON (2022). https://doi.org/10.1007/s12633-022-01865-7
46. T. Simonson, D. Perahia, Comput. Phys. Commun. **91**, 291–303 (1995). https://doi.org/10.1016/0010-4655(95)00054-J
47. M. Amin, J. Küpper, Chem Open **9**, 691–694 (2020). https://doi.org/10.1002/open.202000108
48. A. Cuervo, P.D. Dans, J.L. Carrascosa, M. Orozco, G. Gomila, L. Fumagalli, Proc. Natl. Acad. Sci. U. S. A. **111**, 2 (2014). https://doi.org/10.1073/pnas.1405702111
49. H. Im, X.J. Huang, B. Gu, Y.K. Choi, Nat. Nanotechnol. **2**, 430 (2007). https://doi.org/10.1038/nnano.2007.180